Batteries & Supercaps

Research Article
doi.org/10.1002/batt.202400427

Chemistry Europe
European Chemical Societies Publishing

www.batteries-supercaps.org

Constructing High-Performance Zn-Iodine Batteries with CuI-PVP Composite Layer Coated Zn Anodes

Rui Zhang[+],[a, b] Xiangyu Liu[+],[b] Xiaojing Wu,[b] Tan Guo,*[a] Shan Yun,[a] Lingyu Du,[b] and Litao Kang*[b]

Aqueous zinc-iodine (Zn-I_2) batteries featuring abundant raw materials, inherent safety, excellent cost competitiveness and environmental benignity have been identified as one kind of important electrochemical energy storage devices. However, these batteries always suffer from inferior electrochemical performance, because of dendrite growth and corrosion/passivation of the anodes. Herein, a copper iodide-polyvinylpyrrolidone (CuI-PVP) composite layer is proposed to suppress the parasitic reactions and protect the Zn anodes. In this layer, the CuI can spontaneously react with metallic Zn and convert into Cu and Cu_5Zn_8 ($2CuI + Zn \rightarrow 2Cu + ZnI_2$; $5Cu + 8Zn \rightarrow Cu_5Zn_8$). The highly zincophilic Cu and Cu_5Zn_8, as heterogeneous seeds, can guide the uniform Zn nucleation and deposition, while alleviating corrosion of the Zn anodes. At the same time, the iodide species releasing from the composite layer can be oxidized and deposited on the cathodes, contributing additional capacity. As a result, the symmetric cell prepared with the CuI-PVP@Zn anodes demonstrates a long cycling lifetime of 1400 hours at 1 mA cm^{-2} and 1 mAh cm^{-2}. Under an even higher current density of 5 mA cm^{-2}, the CuI-PVP@Zn cell can still stably work for more than 660 hours. The practical application of this CuI-PVP@Zn electrode has been further demonstrated in Zn-I_2 full batteries, which achieve 60% higher specific capacity than the untreated ones (251.4 vs. 157.1 mAh g^{-1} after 2800 cycles).

1. Introduction

Recently, Zn-iodine (Zn-I_2) batteries have attracted tremendous attentions, thanks to their admirable advantages including raw material abundance, low cost, inherent safety, environmental benignity and fast reaction kinetics.[1–3] The superior electrochemical performance of Zn-I_2 batteries stems from the rational battery chemistry design: (1) Both the I_2 cathodes and Zn anodes undergo dissolution-deposition reactions with high theoretical charge storage capacities (211 and 819 mAh g^{-1}, respectively)[4,5]; (2) The cathodes and the anodes have quite different redox potentials (0.54 and −0.763 V *vs.* SHE, respectively), leading to a noteworthy battery output voltage; (3) The I_2 cathodes are highly reversible and durable, since there is no any irreversible by-product formed during the cathodic reaction; (4) Aqueous electrolytes are much more conductive (1~10^2 S m^{-1}) than their organic counterparts (10^{-6}~10^{-3} S m^{-1}), adequate to support high-rate charge/discharge; (5) Aqueous batteries are inherently safe since they fundamentally eliminate the use of flammable organic electrolytes.[6] Therefore, the combination of Zn anodes and I_2 cathodes in aqueous electrolytes can offer a theoretical energy density of 310 Wh kg^{-1}.

While holding many attractive advantages, commercialization of aqueous Zn-I_2 batteries is seriously hindered by a number of hurdles.[7] Firstly, the I_2 cathodes always suffer from polyiodide shuttle issues. In aqueous Zn-I_2 batteries, there are at least two iodide shuttle mechanisms:

1) I_2 itself is slightly soluble in aqueous electrolytes. This process can be expressed as[8–10]:

$$I_2 + H_2O \leftrightarrow I^- + H^+ + HIO \quad (1.1)$$

2) The discharge product of I_2 cathodes, I^-, can significantly increase the solubility of I_2 via complexation reaction:

$$I_2 + I^- \leftrightarrow I_3^- \quad (1.2)$$

$$I_2 + I_3^- \leftrightarrow I_5^- \quad (1.3)$$

The dissolved polyiodides in the electrolytes can easily cross over routine porous separators (e.g., glass fiber or polypropylene separators), leading to severe self-discharge via reaction with the Zn anodes[11–13]:

$$I_3^- + Zn \rightarrow Zn^{2+} + 3I^- \quad (1.4)$$

Apart from the cathode-related issues, the Zn anodes are also plagued by serious parasitic reactions, such as dendrite growth, hydrogen evolution corrosion, and surface passivation.[14] Dendrite growth on Zn anodes is primarily caused by the "tip

[a] R. Zhang,[+] T. Guo, S. Yun
Jiangsu Provincial Key Laboratory of Palygorskite Science and Applied Technology, Huaiyin Institute of Technology, Huaian 223003, P. R. China
E-mail: guotan@hyit.edu.cn

[b] R. Zhang,[+] X. Liu,[+] X. Wu, L. Du, L. Kang
College of Environment and Materials Engineering, Yantai University, Yantai 264005, China
E-mail: kanglitao@ytu.edu.cn

[+] R. Zhang and X. Liu contributed equally to this work and should be considered as co-first authors.

Supporting information for this article is available on the WWW under https://doi.org/10.1002/batt.202400427

effect", a scientific terminology describing the phenomenon that protrusions with larger surface curvature accumulate higher surface charge density and stronger local electric field intensity.[6,15] The "tip effect" drives preferential Zn^{2+} accumulation to the vicinities of protrusions, stimulating uneven dendritic Zn deposition.[16] The growing dendrites, in turn, amplify the "tip effect" and ultimately lead to a vicious cycle.[17,18] Zn dendrites can cause short-circuit failure in an unpredictable manner by piercing through the separators. In addition, the accumulated Zn dendrites on the anodes are always fluffy, and tend to increase interface impedance and degrade electrochemical performance.[19,20]

Furthermore, Zn anodes are thermodynamically unstable in aqueous electrolytes. According to the Nernst equation, the hydrogen evolution potential of a mildly-acidic electrolyte (pH = 4) is −0.24 V, while the redox potential of Zn is −0.88 V. It means that the metallic Zn can be attacked and corroded in aqueous media.[14] In $ZnSO_4$ electrolytes, the corrosion reaction can be expressed as:

$$4Zn + SO_4^{2-} + 13H_2O \rightarrow Zn_4(OH)_6SO_4 \cdot 5H_2O + 2OH^- + 4H_2 \quad (1.5)$$

Zn corrosion not only consumes electrolytes, but also produces inert by-products. The accumulation of by-products on the surfaces of the Zn anodes may further accelerate dendrite growth, due to the uneven surface passivation and the reduction of Zn deposition sites.[21,22] In addition, the hydrogen gas by-product may lead to battery swelling and/or burst.

To address the aforementioned issues, a variety of innovative strategies has been explored, including electrolyte formulation,[23–25] separator design,[26,27] and anode modification.[19,28,29] In Zn-I_2 batteries, the side reactions mainly occur at the electrolyte/anode interfaces. Therefore, modifying the Zn anodes with functional layers should be one of the most direct and effective approaches to addressing the issues.[30] Significantly, metallic Cu and Cu–Zn alloys not only possess good conductivity and affordable cost, but also exhibits high chemical stability and excellent Zn affinity. Therefore, decorating Zn anodes with Cu and Cu–Zn alloy layer can facilitate uniform Zn nucleation/deposition while suppressing the parasitic reactions. Usually, the Cu and Cu–Zn layers are prepared by thermal evaporation,[31] magnetron sputtering,[32] or the replacement reactions between Zn and copper salt solutions ($CuSO_4$,[33] $CuCl_2$[34]). However, thermal evaporation and magnetron sputtering are time-/energy-consuming due to the requirement of vacuum environment and/or high heating temperature (≥1000 °C). On the other hand, the replacement reactions between Cu^{2+} and metallic Zn are always too fast to control. Figure S1 depicts the photographs of several Zn discs after reacting with $CuCl_2$ aqueous solution. It was found that violent reaction immediately occurred once the Zn discs touched the solution, producing lots of reddish-brown metallic Cu precipitation. After 3 min, the zinc discs were removed out from the solution, and all they were covered by an uneven Cu deposited layer.

In this paper, cuprous iodide (CuI) is used as copper source to prepare the Cu-based protective layer. CuI is hardly soluble in water (solubility = 4.2×10^{-4} g/L), and can therefore enable a much milder solid-state replacement reaction with metallic Zn.

$$2CuI + Zn \rightarrow 2Cu + ZnI_2 \quad (1.6)$$

After reaction, the released I^- from the soluble ZnI_2 can be oxidized and deposited onto the cathodes in the consequent charge process, providing additional capacity.

To ensure a firm contact between CuI nanoparticles and the Zn anodes, polyvinylpyrrolidone (PVP) is further introduced as a binder. PVP is a famous synthetic polymer with exceptional binding and film forming properties, and can therefore greatly increase the adhesion of the coating to the Zn substrates, ensuring high film uniformity and long-term stability.[35] The polar groups of PVP (C=O and N–H), as cation hopping sites, may further promote the uniform Zn^{2+} migration and Zn deposition.[35,36] Thanks to these merits, the CuI-PVP@Zn symmetric cell achieved a long cycling lifetime of 1450 h at 1 mA cm^{-2} and 1 mAh cm^{-2}, 12 times longer than the bare Zn cell (failed after only 120 h). At an even higher current density of 5 mA cm^{-2}, the CuI-PVP@Zn cell could still stably work for more than 660 h. In Zn–I_2 batteries, adoption of the CuI-PVP@Zn anodes enables a high specific capacity of 251.4 mAh g^{-1} at 1 A g^{-1} after 2800 cycles, 60% higher than that of the Zn-anode batteries (157.1 mAh g^{-1}).

Experimental Section

Preparation of CuI-PVP Coated Zn Foils (CuI-PVP@Zn)

All solvents and chemicals are of reagent grade and used as received without further purification. Firstly, 0.6 g of polyvinylpyrrolidone (PVP, 300,000) was dissolved in 2.5 ml deionized water by 12 hours stirring. Afterwards, 3.1 g of cuprous iodide (CuI) was added to the PVP solution, and then stirred for another 12 hours to obtain the coating slurry. Finally, the CuI-PVP slurry was spin-coated on the Zn foils (2.5 cm×2.5 cm, 100 μm in thickness) at 5000 rpm for 30 seconds. The Zn foils were then dried at room temperature for 12 hours, and finally cut into discs (Φ16 mm). It should be noted that although PVP is soluble in water, it is difficult to dissolve in the employed 2.7 m $ZnSO_4$ (molality, i.e., 2.7 mol kg^{-1}) electrolyte. As shown in Figure S2, the PVP solution (0.68 g L^{-1} PVP in10 mL water, equivalent to the PVP weight in a CuI-PVP@Zn electrode) manifests a strong PVP characteristic absorbance peak at 200–250 nm, while the PVP peak is undetectable in the $ZnSO_4$ electrolyte after soaking a CuI-PVP@Zn electrode for 7 days. Similar experimental phenomena have also been reported previously.[37]

Preparation of I_2@AC Cathodes

An thermal-assisted I_2-infiltrating method was used to prepare the I_2@AC composite.[13,38] Firstly, 0.5 g I_2 and 0.5 g activated carbon (AC) were thoroughly mixed by grinding. Then, the mixed powder was transferred into a 50 mL Teflon-line stainless autoclave and heated at 90 °C for 4 h, during which the I_2 was sublimated and infused into the pores of the AC host. After natural cooling, the porous carbon enveloped I_2 (I_2@AC) composite was obtained. In the I_2@AC composite, the iodine content was determined to be 48 wt% by thermogravimetry analysis (TGA).[39] To prepare the cathode coatings, the I_2@AC composite powder (active material) was mixed

Research Article
doi.org/10.1002/batt.202400427
Chemistry Europe
European Chemical Societies Publishing

with acetylene black (conductive agent) and polyvinylidene difluoride (PVDF, binder) with a mass ratio of 7:2:1 in the proper amount of N-methyl pyrrolidone (NMP, solvent). Then, the resulting slurry was uniformly coated onto graphite papers (current collector) with average I_2 mass loading of about 1.5~2 mg cm^{-2}. After 12 h drying at 40 °C, the I_2@AC coated GPs were cut into Φ16 mm discs.

Material Characterization

The X-ray diffraction (XRD) measurement was carried out on a D/max-2500/PC X-ray diffractometer using Cu Kα radiation (λ = 0.1542 nm) from 30~80°. Surficial morphologies and elemental mapping images of the samples were characterized by a JEOL JSM-7610F field emission scanning electron microscope (SEM) equipped with an energy-dispersive spectroscope (EDS). Wettability of the electrolyte (10 μl, 2.7 m $ZnSO_4$) on the anodes was measured by using an optical contact angle and interfacial tension meter (CA, CA100 C, Innuo, China) under room temperature in air. The UV-vis absorption spectra were collected on a Persee TU-1810 UV-Vis spectrophotometer within a wavelength range of 190~600 nm.

Electrochemical Measurements

To investigate the influence of the CuI-PVP composite layers on electrochemical performances, different type of CR-2032 button cells were assembled with 2.7 m $ZnSO_4$ aqueous electrolyte (120 μL), glass fiber paper separators (Φ19 mm, Whatman), and various electrodes (bare Zn anode, CuI-PVP@Zn anodes, I_2@AC cathodes, bare Ti/Cu/stainless steel (SS) discs, Ti/Cu/SS discs with CuI-PVP coating). Galvanostatic charge-discharge (GCD) tests were performed on LAND-CT2001 A battery-testing instrument. Cyclic voltammetry (CV), electrochemical impedance spectroscopy (EIS), chronoamperometry (CA), Tafel, and Linear sweep voltammetry (LSV) tests were performed on a CHI-660E electrochemical workstation. The CV, EIS, and CA tests were carried out in a two-electrode configuration, while the Tafel and LSV tests in a three-electrode configuration (Ti foil and Ag/AgCl were adopted as counter and reference electrodes, respectively). In the LSV test, K_2SO_4 electrolyte instead of $ZnSO_4$ electrolyte was used to exclude the interference from the Zn plating reaction.

2. Results and Discussion

The CuI-PVP composite layers were prepared by a spin-coating method. In these layers, both CuI and PVP was initially colorless (Figure S3). Nevertheless, the composite layer gradually changed into black after coating on the Zn discs (inset in Figure 1a), indicating the occurrence of the replacement reaction between the CuI and the metallic Zn substrate (**Equation (1.6)**). In the XRD pattern of the CuI-PVP@Zn, XRD peaks of ZnI_2, Cu, and Cu_5Zn_8 were detected besides some minor CuI peaks, suggesting that the majority of CuI had been reduced into metallic Cu and Cu_5Zn_8. DFT studies have shown that both Cu and Cu_5Zn_8 are highly zincophilic,[32] and can therefore work as heterogeneous seeds to guide the uniform Zn nucleation and deposition.[40,41]

Figure 1b shows the surficial morphology of the Zn and CuI-PVP@Zn anodes. The bare Zn anode showed a dense and flat surface with parallel hot-pressing indentations, which are one of the underlying reasons triggering Zn dendrite growth.[42] After coating, a uniform porous layer with a thickness of ~25 μm is observed on the top surface of the Zn anode (Figure S4). EDS mapping images indicate that the Cu, Zn, and N elements are uniformly distributed in the layer, confirming the thorough mixture of the CuI and PVP components (Figure 1c). Thanks to the hydrophility of the PVP component,[43] the CuI-PVP@Zn anode exhibited much better electrolyte wettability compared to the bare Zn anode (contact angle: 36° *vs.* 81°, Figure S5), favorable to enhance the anode/electrolyte contact and Zn striping/plating kinetics.

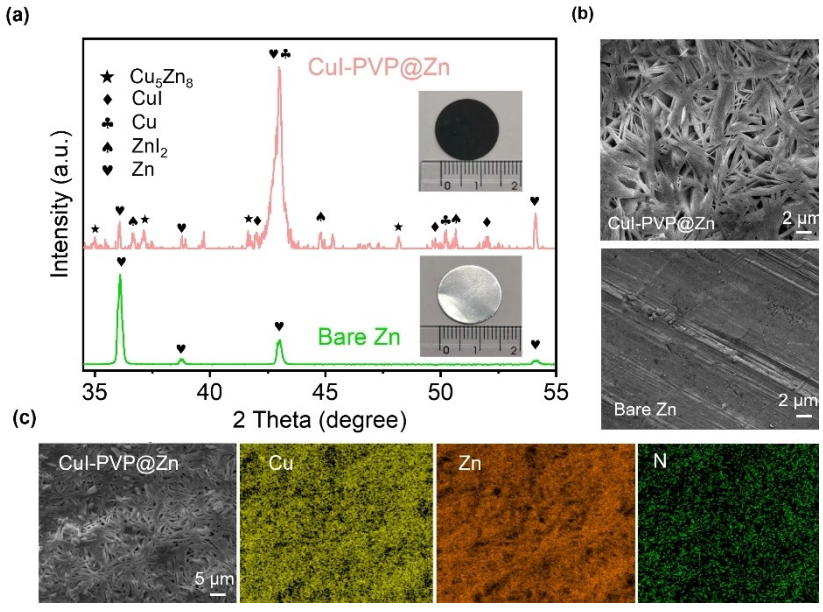

Figure 1. (a) XRD patterns, photographs (insets), and (b) SEM images of a bare Zn and a CuI-PVP@Zn anode. (c) Elemental mapping images of a CuI-PVP@Zn anode.

Research Article
doi.org/10.1002/batt.202400427
Chemistry Europe
European Chemical Societies Publishing

To investigate the influence of the CuI-PVP layer on electrochemical performance, a series of symmetric cells was assembled with bare Zn or CuI-PVP@Zn anodes. Running at 1 mA cm^{-2} and 1 mAh cm^{-2}, the bare Zn cell suddenly failed after only 120 h (Figure 2a). In contrast, the CuI-PVP@Zn symmetric cell worked stably within 1450 h before the dramatic increase of polarization. Longer lifetime of the CuI-PVP@Zn cells is highly reproducible. For instance, the CuI-PVP@Zn cell achieved a lifetime of 727 h at 3 mA cm^{-2} and 3 mAh cm^{-2}, while the Zn cell failed after only 55 h (Figure 2b). Under even harsher testing condition of 5 mA cm^{-2} and 5 mAh cm^{-2}, the CuI-PVP@Zn cell still achieved a noteworthy lifetime of 665 h, 21 times longer than that of the Zn cell (31 h, Figure 2c). Figure 2d further shows the rate performance of the symmetric cells. At current densities $\leq$1 mA cm^{-2}, the CuI-PVP@Zn cell exhibited obviously lower polarization voltages than the Zn cell, thanks to the highly zincophilicity of the protective layer.[42] More importantly, the CuI-PVP@Zn cell could easily pass the test. In striking contrast, the Zn cell underwent obvious polarization voltage fluctuations within 280~320 h. Afterwards, the voltage profile changed into a square wave curve, suggesting shorting failure of this cell.[44] As shown in Table S1 and Figure S6, cycling stability of the CuI-PVP@Zn anode is comparable or even superior to the reported data.

Figure 3a further shows the Coulombic efficiencies (CEs) of Zn–Cu asymmetric cells with different Cu electrodes. In the initial dozens of cycles, the CuI-PVP@Cu cell exhibited slightly lower CEs, due to the consumption of plated Zn by the residual CuI (Figure 1a and **Equation (1.6)**). Afterwards, the cell worked steadily for 590 cycles with an average CE of 98.02%. By comparison, the bare Cu cell only survived for 36 cycles with an average CE of 97.99%. Figure 3b–c further demonstrates the Zn striping/plating voltage profiles of these asymmetric cells. The unstable voltage profiles of the bare Cu cell clearly reflect the poor Zn plating/striping stability. Whereas, the CuI-PVP@Cu cell shows smooth and stable voltage curves, highlighting higher Zn plating/striping stability. The improved Zn plating/striping stability was also observed in Zn–Ti and Zn-SS (stainless steel) asymmetric cells. The CuI-PVP@Ti cell worked steadily for 500 cycles, and manifested a much higher average CE (97.86% vs. 84.00%, Figure S7a–c). The CuI-PVP@SS cell achieved a lifetime of over 300 cycles with an average CE of 96.49%; while the bare SS cell short-circuited after only 13 cycles with an average CE of only 47.99% (Figure S7d–f).

Figure 3d displays chronoamperometry (CA) curves of the symmetric cells with Zn and CuI-PVP@Zn anodes, which can accurately reflect surface changes of the electrodes during Zn plating.[45] At a constant potential of −150 mV, the current density of the Zn cell increased continuously within the test period, representing fast dendrite growth on the electrode surface.[46] The growing dendrite captured the migrating Zn^{2+} ions and forbade them from vertical diffusion, leading to a longer 2D Zn^{2+} diffusion process.[37] Different from the Zn cell, 2D diffusion process kept for only ~9 s in the CuI-PVP@Zn cell,

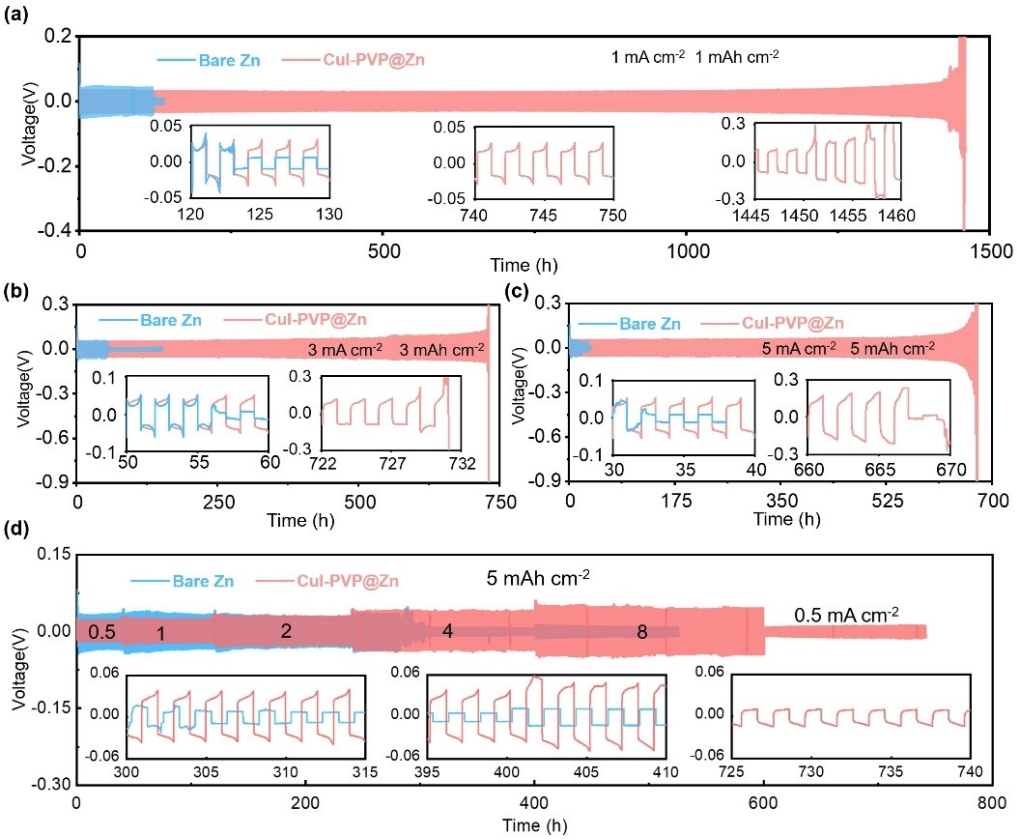

Figure 2. Galvanostatic striping/plating test of the bare Zn and CuI-PVP@Zn electrodes in symmetric cells under the conditions of (a) 1 mA cm^{-2}, 1 mAh cm^{-2}; (b) 3 mA cm^{-2}, 3 mAh cm^{-2}; (c) 5 mA cm^{-2}, 5 mAh cm^{-2}. (d) Rate performance of these cells at stepwise changing current densities.

Research Article
doi.org/10.1002/batt.202400427
Chemistry Europe
European Chemical Societies Publishing

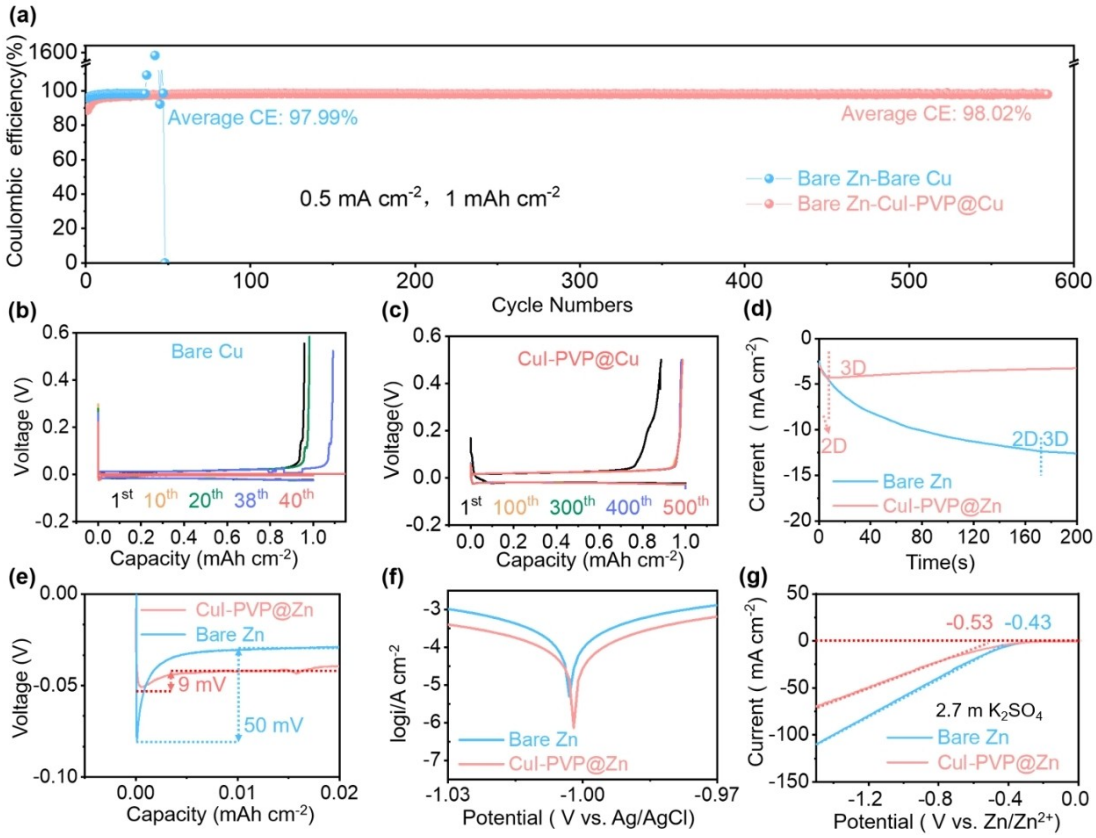

Figure 3. (a) Coulombic efficiencies (CEs) and (b–c) voltage profiles of Zn–Cu and Zn-CuI-PVP@Cu cells under the conditions of 0.5 mA cm^{-2} and 1 mAh cm^{-2}. (d) Chronoamperometry curves of Zn and CuI-PVP@Zn symmetric cells at an applied voltage of −150 mV. (e) The initial deposition process of symmetric cells at a current density of 5 mA cm^{-2}. (f) Tafel and (g) LSV curves of Zn and CuI-PVP@Zn electrodes.

followed by a long and stable 3D diffusion process, suggesting an uniform Zn deposition process on the CuI-PVP@Zn electrode.[47] Figure 3e manifests the initial voltage evolution curves of a bare Zn and a CuI-PVP@Zn electrode. The bare Zn electrode needed a large overpotential of 50 mV to drive the nucleation of Zn deposits, while the CuI-PVP@Zn electrode needed only 9 mV. The overpotential reduction can be attributed to the formation of zincophilic Cu and Cu_5Zn_8 in the layer, which can effectively reduce the nucleation energy barrier and improve Zn deposition uniformity.[32] Moreover, the CuI-PVP@Zn cells also exhibit smaller charge transfer resistance (Rct, Figure S8), suggesting better Zn stripping/plating kinetics.[41,48]

Figure 3f presents the Tafel curves of a bare Zn and a CuI-PVP@Zn electrode. The corrosion current of the Zn electrode decreased from 1.377 mA cm^{-2} down to 0.613 mA cm^{-2} after the coating the CuI-PVP protective layer, indicating a significant reduction of Zn corrosion rate. Figure 3g further depicts the linear sweep voltammetry (LSV) curves of these electrodes in 1 mol/L K_2SO_4 electrolyte. The CuI-PVP@Zn electrode demonstrated higher HER overpotential than the Zn electrode (−0.53 V *vs.* −0.43 V, Ag/AgCl), confirming the effectiveness of the protective layer on inhibiting hydrogen evolution reaction. Figure S9 further displays typical photical micrographs of a Zn and a CuI-PVP@Zn electrode during Zn plating. Within 90 minutes, the CuI-PVP@Zn electrode kept bubble-free while visible bubbles began to appear on the surface of the Zn electrode. 100 minutes later, small bubbles began to appear on the surface of the CuI-PVP@Zn electrode, but with still an obviously slower evolution rate.

To reveal the Zn striping/plating behavior, the cross-sectional SEM images of the cycled electrodes are further collected. As shown in Figure 4a–b, the top surface of the bare Zn anode became obviously rough and bumpy after the cycling test, indicating an uneven Zn striping/plating process. On contrary, the CuI-PVP@Zn anode remained a flat and dense surface and a distinct top layer after the cycling test, indicating a uniform Zn striping/plating process (Figure 4c–d). Figure 4e graphically summarizes the deposition processes of the bare Zn and CuI-PVP@Zn electrode. The bare Zn electrode suffers from rapid hydrogen evolution corrosion reaction during cycling. The corrosion-induced uneven passivation, along with the manufacturing deficiencies, trigger dendritic Zn deposition and instable Zn striping/plating process. After coating the CuI-PVP layer, the generated Cu and Cu_5Zn_8 ensure a much more uniform Zn nucleation and deposition process, thanks to their high zincophilities and strong Zn atom adsorption capacity.[32] Moreover, the abundant polar groups (C=O and N–H) of the PVP component, working as the hopping sites, are helpful to further homogenize the Zn migration.[35]

Research Article
doi.org/10.1002/batt.202400427
Chemistry Europe
European Chemical Societies Publishing

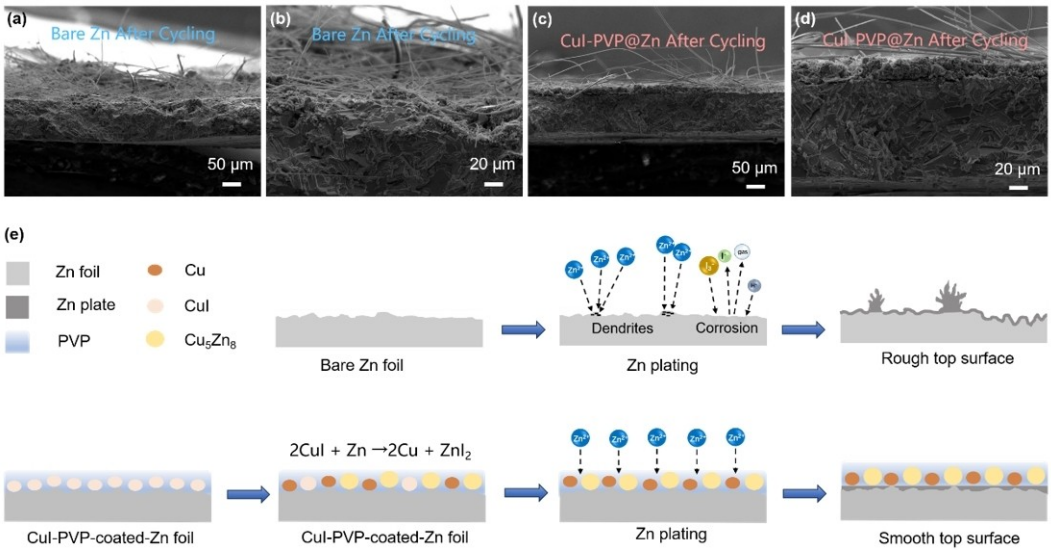

Figure 4. (a–d) Cross-sectional SEM images of a CuI-PVP@Zn (a,b) and bare Zn (c,d) anode after cyclic test under 1 mA cm^{-2} and 1 mAh cm^{-2} for 100 h. (e) Schematic diagram showing the different Zn striping/plating process of the bare Zn and CuI-PVP@Zn electrodes.

To demonstrate the practical application feasibility of the CuI-PVP@Zn anodes, Zn-I_2 full batteries were assembled with I_2@AC cathodes, 2.7 m $ZnSO_4$ electrolyte, and different anodes. The CuI-PVP@Zn battery achieved a larger capacity and smaller polarization voltage than the bare Zn one (Figure 5a–b). The smaller polarization voltage can be attributed to the improved Zn striping/plating kinetics enabled by the CuI-PVP protective layer. On the other hand, the larger capacity comes from the extra capacity contribution from the CuI-induced iodine. After coating, the CuI component was converted into highly-zincophilic Cu/Cu_5Zn_8 and soluble ZnI_2 (**Equation (1.6)**). The dissolved I^- from ZnI_2 was oxidized into I_2 on the cathode side and provided additional capacity. To verify this hypothesis, an equivalent amount of KI was directly added into the electrolyte. As shown in Figure S10, the KI-modified electrolyte remarkably boosted the battery's capacities, due to the additional capacity provided by the KI additive.

Rate performance test indicates that the CuI-PVP@Zn battery outputted higher capacities regardless of the current densities (Figure 5c). For example, the CuI-PVP@Zn battery delivers 1.6 times larger capacity than the bare Zn battery at 0.1 A g^{-1} (313.7 *vs.* 189.7 mAh g^{-1}). At 5 A g^{-1}, the capacity of CuI-PVP@Zn battery is still much higher than that of the bare Zn battery (243.6 *vs.* 134.5 mAh g^{-1}). Figure 5d further manifests the cycling performance of these batteries. At 1 A g^{-1}, the CuI-PVP@Zn battery delivered a capacity of 354 and 251.4 mAh g^{-1} at the 1st and 2800th cycle, respectively, with an average coulombic efficiency of 99.86%. As a comparison, the bare Zn

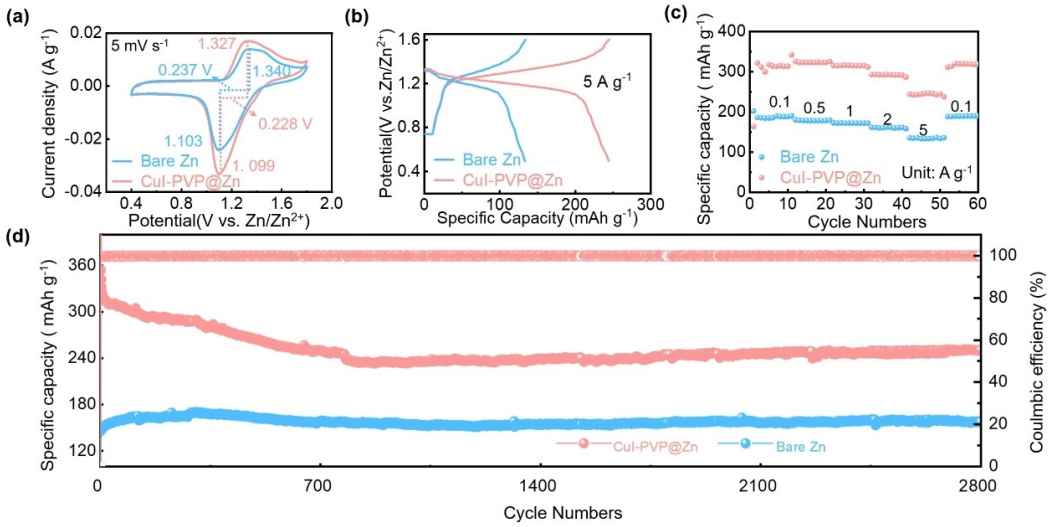

Figure 5. Electrochemical performance of Zn-I_2 batteries with bare Zn or CuI-PVP@Zn anodes: (a) CV curve at 5 mV s^{-1}, (b) voltage profiles at 5 A g^{-1}, (c) rate performance from 0.1–5 A g^{-1} and (d) cycling performance at 1 A g^{-1}.

battery provided much lower capacities (147.1 and 157.1 mAh g^{-1}, respectively) and a slightly lower average coulombic efficiency (99.69 %). The rapider capacity decay of the CuI-PVP@Zn battery can be ascribed to the low actual AC:I_2 mass ratio in this battery. As mentioned above, iodine in the CuI can be deposited on the I_2@AC cathode and contribute additional capacity during battery charging. This change will definitely reduce the AC:I_2 mass ratio, thereby reducing the conductivity and iodide limitation of the electrode.[13] We believe that this should be the reason for the rapid capacity decay. To verify this speculation, we prepared three I_2@AC active materials with different AC:I_2 mass ratios (1 : 1; 1 : 2; 1 : 3) and tested their cycling performance at a current density of 1 A/g^{-1} (Figure S11). As expected, the cycling stability of these materials decreased with the decrease of AC:I_2 mass ratio, thus verifying our speculation.

3. Conclusions

In summary, a uniform CuI-PVP composite layer was coated on Zn anodes by spin-coating. In the coating, the CuI can spontaneously react with the Zn anodes, producing highly zincophilic Cu and Cu_5Zn_8, which can guide even Zn nucleation/deposition as heterogeneous seeds. While the polar groups (C═O and N–H) in PVP provided abundant hopping sites to homogenize the Zn^{2+} flux. Thanks to the high stability of Cu, Cu_5Zn_8 and PVP, this coating can also suppress hydrogen evolution and Zn corrosion reactions. At the same time, the released iodide species from the coating can provide additional capacities. As a result, the CuI-PVP@Zn electrode achieved much better Zn striping/plating stability than the bare Zn electrode, in both symmetric cell and full batteries. This CuI-PVP coating strategy circumvent the difficulties encountered by the thermal evaporation and solution-based replacement reaction possesses, providing a new approach for the modification of Zn anodes.

Acknowledgements

The authors thank the Open Foundation of Key Laboratory for Palygorskite Science Applied Technology of Jiangsu Province (HPK202103), the National Natural Science Foundation of China (22309159, 51502194), the Natural Science Foundation of Shandong (ZR2023QB184, ZR2020ME024) for financial support.

Conflict of Interests

The authors declare no conflict of interest.

Data Availability Statement

The data that support the findings of this study are available on request from the corresponding author. The data are not publicly available due to privacy or ethical restrictions.

Keywords: Zn iodine battery · Zn anode · CuI · PVP · Cu

[1] K. K. Turekian, K. H. Wedepohl, *Geol. Soc. Am. Bull.* **1961**, *72*(2), 175–192.
[2] D. Kundu, et al., *Nat. Energy* **2016**, *1*(10), 1–8.
[3] M. Winter, R. J. Brodd, *Chem. Rev.* **2004**, *104*(10), 4245–4270.
[4] H. Jia, et al., *Nano Energy* **2020**, *70*, 104523.
[5] Y. Liu, et al., *Adv. Funct. Mater.* **2021**, *31*(13), 2010445.
[6] Q. Yang, et al., *Adv. Mater.* **2019**, *31*(43), 1903778.
[7] D. Yu, et al., *ACS Sustainable Chem. Eng.* **2020**, *8*(36), 13769–13776.
[8] V. T. Calabrese, A. Khan, *J. Polym. Sci., Part A: Polym. Chem.* **1999**, *37*(15), 2711–2717.
[9] J. A. Rendleman Jr, *Carbohydr. Polym.* **2003**, *51*(2), 191–202.
[10] H. Wang, et al., *Small* **2024**, *20*(13), 2306947.
[11] L. Yan, et al., *Carbon* **2022**, *187*, 145–152.
[12] Q. Zhao, et al., *Nano Lett.* **2015**, *15*(9), 5982–5987.
[13] W. Li, K. Wang, K. Jiang, *J. Mater. Chem. A* **2020**, *8*(7), 3785–3794.
[14] L. Ma, et al., *Adv. Mater.* **2020**, *32*(14), 1908121.
[15] J. Barton, J. O. M. Bockris, *Proc. R. Soc. London. Ser. A. Math. Phys. Sci.* **1962**, *268*(1335), 485–505.
[16] W. Zhang, et al., *Sci. Adv.* **2018**, *4*(2), eaar4410.
[17] L. Gireaud, et al., *Electrochem. Commun.* **2006**, *8*(10), 1639–1649.
[18] G. Yasin, et al., *Energy Storage Mater.* **2020**, *25*, 644–678.
[19] Z. Yi, et al., *Adv. Energy Mater.* **2021**, *11*(1), 2003065.
[20] L. N. Bengoa, et al., *J. Mater. Eng. Perform.* **2018**, *27*, 1103–1108.
[21] H. Pan, et al., *Nat. Energy* **2016**, *1*(5), 1–7.
[22] J. Hao, et al., *Energy Environ. Sci.* **2020**, *13*(11), 3917–3949.
[23] J. Zhao, et al., *Nano Energy* **2019**, *57*, 625–634.
[24] K. E. Sun, et al., *ACS Appl. Mater. Interfaces* **2017**, *9*(11), 9681–9687.
[25] F. Wang, et al., *Nat. Mater.* **2018**, *17*(6), 543–549.
[26] Y. Zong, et al., *Adv. Energy Mater.* **2023**, *13*(20), 2300403.
[27] J. Chen, et al., *Energy Rev.* **2022**, *1*(1), 100005.
[28] C. Zhu, et al., *Coord. Chem. Rev.* **2023**, *485*, 215142.
[29] Y. Zhu, et al., *Energy Environ. Sci.* **2024**, *17*(2), 369–385.
[30] W. Shang, et al., *Nano-Micro Lett.* **2022**, *14*(1), 82.
[31] Y. Zhang, et al., *Chem. Eng. J.* **2021**, *416*, 128062.
[32] B. Li, et al., *Angew. Chem.* **2022**, *134*(47), e202212587.
[33] C. Liu, et al., *Nanomaterials* **2021**, *11*(3), 764.
[34] Z. Cai, et al., *Energy Storage Mater.* **2020**, *27*, 205–211.
[35] Z. Li, et al., *J. Mater. Chem. A* **2020**, *8*(34), 17725–17731.
[36] Q. Shen, et al., *Sci. China Mater.* **2024**, *67*, 2266–2276.
[37] Y. Zhang, et al., *Nano-Micro Lett.* **2022**, *14*(1), 208.
[38] C. Bai, et al., *Nano Res.* **2018**, *11*, 3548–3554.
[39] G. Chen, et al., *Chem. Eng. J.* **2020**, *401*, 126065.
[40] B. Li, et al., *Angew. Chem. Int. Ed. Engl.* **2022**, *61*(47), e202212587.
[41] M. Cui, et al., *ACS Appl. Energy Mater.* **2019**, *2*(9), 6490–6496.
[42] S.-S. Liu, et al., *Rare Met.* **2024**, *43*, 2125–2135.
[43] B. Macdonald, et al., *ACS Appl. Mater. Interfaces* **2024**, *16*(10), 13018–13028.
[44] Q. Li, et al., *Joule* **2022**, *6*(2), 273–279.
[45] Y. Lin, et al., *Energy Environ. Sci.* **2023**, *16*(2), 687–697.
[46] J. Park, et al., *Adv. Mater.* **2020**, *32*(4), 1904411.
[47] G. Trejo, et al., *J. Appl. Electrochem.* **2001**, *31*, 685–692.
[48] G. Yasin, et al., *ACS Catal.* **2023**, *13*(4), 2313–2325.

Manuscript received: June 28, 2024
Revised manuscript received: September 14, 2024
Accepted manuscript online: October 10, 2024
Version of record online: November 14, 2024